COBEM 2021 26th International Congress of Mechanical Engineering
November 22-26, 2021, Virtual Congress, Brazil

COB-2021-1255
NUMERICAL-EXPERIMENTAL INVESTIGATION OF CRYOPRESERVATION PROCESS BY DROPLET VITRIFICATION

Álisson Renan Stochero da Silva
alissonstochero@hotmail.com
Jacqueline Biancon Copetti
jcopetti@unisinos.br
Mário Henrique Macagnan
mhmac@unisinos.br
Guilherme Dahmer Steffenon
guilhermesteffenon@gmail.com
Massoxi Mandela Cuieca
massoxymandela@hotmail.com
University of Vale do Rio dos Sinos, 950 Unisinos Avenue, São Leopoldo, 93022-750, RS, Brasil

Abstract. *The vitrification of biological materials is a segment of cryopreservation that aims the ultrafast freezing of a cell sample, through the direct transition from a liquid state to a vitrified and amorphous state, without the occurrence of crystallization, reaching cooling rates in the order of 37.000 °C/s, depending on the type of protocol to be used. Several studies have emerged in order to develop and improve ultrafast freezing protocols by vitrification, as well as to investigate the governing phenomena of these processes, both in the field of assisted reproduction and in the study of stem cells for the treatment of diseases. In this context, this work aims to investigate numerically and experimentally the phenomena involved during the vitrification process, such as cooling rate, solidification rate and temperature behavior. There were performed 6 experiments obtaining the curves of temperature and values of cooling rates. A good agreement between the numerical result and the experimental results can be seen, with a relative difference of 0.33% for the cooling rate, being 589.92 °C/min and 591.8 °C/min, respectively. The total solidification of the droplet occurred in 9.965 seconds. The maximum difference between the average of the experimental and numerical cooling rate was 30.54%, due to the temperature measurement position and the discrepancy between the experimental and simulated contact angles.*

Keywords: *Cryopreservation, Droplet vitrification, Experimental vitrification, Computational Fluid Dynamics.*

1. INTRODUCTION

The cryopreservation of cells and tissues is a very broad and developing field, with several applications in medicine and experimental biology, such as assisted reproduction, disease treatment, genetic enhancement, conservation of embryos and other biological materials, where research for new methods of cryopreservation and the improvement of existing protocols has fundamental importance for relevant scientific advances in this area. The current cryopreservation methods can be classified into two groups: slow freezing and rapid freezing methods (Bahari *et al*., 2018). Recently, rapid freezing methods have gained greater importance due to their thermal and biological characteristics, where it is possible to achieve high cooling rates and sample viability, reducing or even avoiding the use of cryoprotective agents, which can be toxic, as is the case of DMSO, for example.

Among the rapid freezing methods, we can highlight the ultra-fast freezing segment, also known as vitrification. Vitrification is the passage from a medium in a liquid state to a vitrified and amorphous state, without the occurrence of crystallization (Santin *et al*., 2009). There are several vitrification methods, such as the OPS method (Vajta *et al*., 1998), thin film evaporation (Su *et al*., 2018), film vitrification (Tiersch *et al*., 2020), microencapsulation vitrification (Li *et al*., 2019), directional vitrification (Bahari *et al*., 2018), microchannel vitrification (Zhao and Fu, 2017; Zhou *et al*., 2017 and Han *et al*., 2008), isochoric vitrification (Zhang *et al*., 2018), droplet vitrification (Shi *et al*., 2015; Vries *et al*., 2018; Dupesh *et al*., 2019; Marchesi *et al*., 2005, Akiyama *et al*., 2019) among others.

The droplet vitrification process can be classified into two main methods: by immersion and by contact. The immersion droplet vitrification method is characterized by the direct contact of the sample with the refrigerant, usually liquid nitrogen. This process is widely used and studied due to the simplicity of the process, high cooling rates and sample viability. The contact droplet vitrification process is characterized by the fact that the sample does not has contact with the refrigerant medium, where the droplet is suspended on a surface in contact with the low temperature region.

Dupesh *et al*. (2019) developed a simple and practical system for vitrifying human semen, using the droplet method, as shown in Fig. 1. The proposed system consists of immersing in nitrogen small droplets of semen mixed with a

cryoprotective solution composed of 0.5 M sucrose, with a volume of 30 μL each. The authors achieved good motility rates, above 70% after thawing using their proposed system, without the use of highly toxic cryoprotective substances.

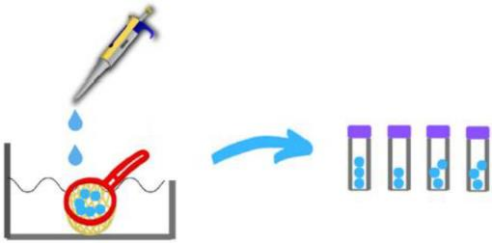

Figure 1. Droplet vitrification by immersion in liquid nitrogen.
Source: Adapted from Dupesch et al. (2019).

Vries *et al*. (2018) also developed a droplet cell vitrification system together with an osmotic dehydration method, using large amounts of cells, where the droplets have direct contact with liquid nitrogen. Figure 2 shows the experimental apparatus proposed by the authors.

Figure 2. Droplet vitrification by immersion proposed by Vries *et al*. (2019).
Source: Adapted from Vries *et al*. (2019).

The authors used large volume of droplets, with diameters of 3 mm and 5 mm, with low percentages of cryoprotective agent (15% by volume), in order to minimize toxicity and loss of sample viability. Cooling rates of 1.320 ºC/min were achieved for droplets with 3 mm in diameter and 960 ºC/min for droplets with 5 mm in diameter, with good viability of metabolic function after thawing.

Shi *et al*. (2015) carried out a numerical and experimental study of contact droplet vitrification, see Fig. 3, in which the droplets are not in contact with liquid nitrogen, without the risk of contamination and with high cooling rates.

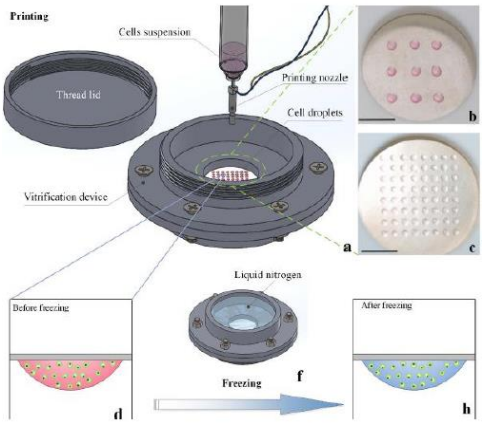

Figure 3. Droplet vitrification by contact proposed by Shi *et al*. (2015).
Source: Adapted from Shi *et al*. (2015).

In this system, droplets are suspended on a silver substrate with 150 μm thick through the effect of surface tension. This thin silver plate is in contact with a reservoir filled with liquid nitrogen, which keeps it constantly cool at extremely low temperatures. The contact angle between the droplets and the conductive surface was 52º, and the droplet diameter

was varied in 0.2 μL, 1 μL and 5 μL. Numerical simulations were performed using COMSOL® software to determine the temperature curve. The authors achieved high cooling rates, approximately 1.146 K/min, reaching a temperature of 120 K around 10 s after the start of the vitrification process. An inhomogeneous crystallization was verified comparing the base of the droplet with its surface, which is expected, due to the difference in heat transfer between the base of the droplet and the silver substrate, which is much higher than the surface of the drop with the environment around it. It was also possible to obtain a good viability rate of the genetic material, with viability of 76% for the case with droplets of 5 μL and 62% for droplets with a diameter of 0.2 μL.

Akiyama *et al*. (2019) also developed a contact droplet vitrification method simulating numerically the proposed system through COMSOL® software. The technique consists of depositing microdroplets on a surface at an extremely low temperature, immersed in liquid nitrogen, achieving extremely high cooling rates, as illustrated in Fig. 4.

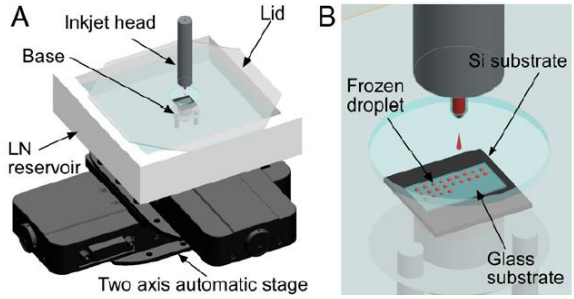

Figure 4. Droplet vitrification by contact proposed by Akiyama *et al*. (2019).
Source: Adapted from Akiyama *et al*. (2019).

The authors achieved cooling rates in the order of $3.7x10^4$ ºC/s, varying only the substrate thickness (150 μm and 5 μm) and the diameter of the dripping nozzle (60 μm and 40 μm), resulting in droplets with a volume of approximately 200 pL and 40 pL. Then, this work will evaluate numerically and experimentally the contact droplet vitrification process, in order to know the phenomena involved during the freezing of the sample, such as temperature curves, cooling and solidification rates. Through computational modeling it will be possible to collect a wide variety of information from the sample and the solidification process, which would not be feasible experimentally.

2. EXPERIMENTAL PROCEDURE

The droplet vitrification experimental bench is composed of a data acquisition system, a video recording system and a vitrification system, as shown in Fig. 5.

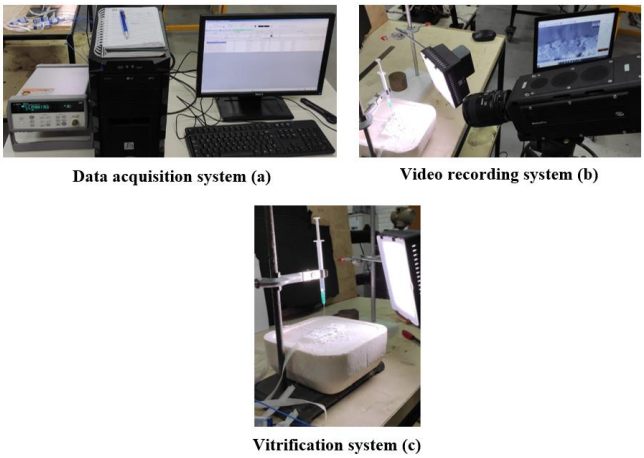

Figure 5: Experimental bench for droplet vitrification.

The data acquisition system, Fig. 5(a), is composed of a computer and a data acquisition module from the Agilent brand, model 34792A, with a 16-channel model 34902A acquisition board (used for thermocouple calibration). A NOVUS brand data acquisition module, Fieldlogger model, with 8 analogic/digital input channels, with data recording capacity of up to 0.001 seconds, is also used to record the temperatures during the experiment. The tests were performed by collecting temperature data every 0.01 seconds, in order to reduce reading fluctuations due to external effects of the experiment.

The video recording system, Fig. 5(b) is composed of a computer and a high-speed camera from the IDT brand, model Motion Pro Y4. The video recording of the tests was carried out with a capture rate of 600 FPS (frames per second). The vitrification system, Fig. 5(c), is composed of a polystyrene vessel for storing liquid nitrogen, a brass cylinder, a syringe with a volume of 1 ml and an opening of 0.7 mm, three thermocouples of the brand Omega type T, used to read the temperature of the drop, the vitrification surface and the environment temperature, and a PT100 calibration thermocouple.

The experimental procedure is carried out as follows: deionized water is collected through a syringe positioned on the freezing/vitrification surface (brass cylinder immersed in liquid nitrogen). Then, a droplet with a volume of approximately 20 µL (O'Neill *et al*., 2019) is dripped over a thermocouple positioned on the freezing surface at approximately 0.5x the droplet diameter. During the experiment, the video recording of the droplet vitrification was carried out through the collection of images from the test plane to measure the contact angle of the droplet with the surface. Figure 6 shows the procedure for determining the contact angle between the droplet and the freezing surface, as well as the values found.

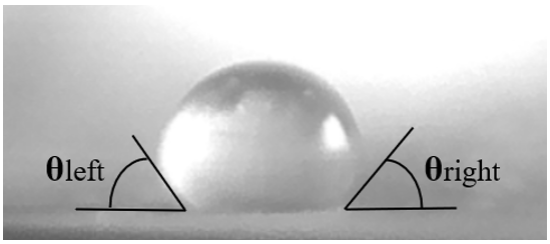

Experimental contact angle			
	Angle - left [°]	Angle - right [°]	Angle average [°]
Droplet 1	52,431	51,843	52,137
Droplet 2	87,797	88,698	88,248
Droplet 3	65,879	65,462	65,671
Droplet 4	64,983	60,642	62,813
Droplet 5	81,416	72,316	76,866
Droplet 6	84,094	81,027	82,561
Droplet 7	84,053	78,518	81,286
Droplet 8	80,022	74,962	77,492
Droplet 9	67,620	67,479	67,550
Droplet 10	75,069	76,651	75,860
Droplet 11	88,238	90,000	89,119

Figure 6. Experimental procedure applied to obtaining the contact angle.

As illustrated in Fig. 6, 11 measurements of the contact angle between the droplet and the freezing surface were performed, obtaining an average angle of 74.51°, with a standard deviation of 11.37°. This large variation in the contact angle is related to the procedure used during the measurements, which is influenced by some factors, such as inclination and drop height, which were not controlled during the tests.

3. NUMERICAL PROCEDURE

The CFD computer simulations were performed using ANSYS Fluent® software, in order to analyze the behavior of the droplet during vitrification, through the temperature and solidification curves. The numerical domain used in the simulations is described in Fig. 7.

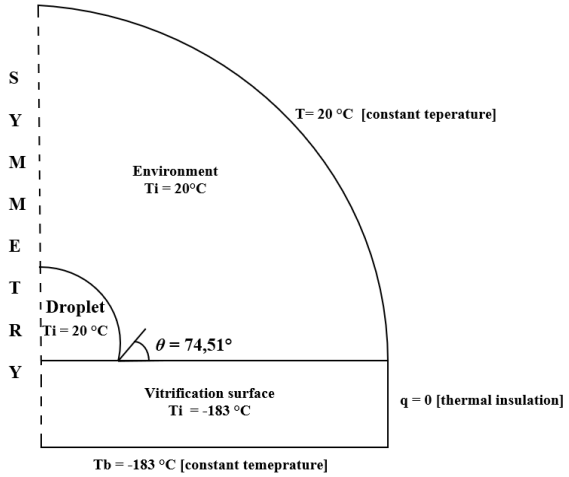

Figure 7. Numerical domain and boundary conditions.

As illustrated in Fig. 7, the numerical domain consists of 3 regions of different materials, the droplet being composed of water, environment (air) and vitrification surface (brass). The initial droplet temperature is the same as the environment 20 °C, while the freezing substrate temperature is -183 °C. The outer regions, such as the bottom surface of the substrate

and the boundaries of the environment, are considered to have a constant temperature, with the end of the brass cylinder considered to be thermally insulated.

The size of the environment was defined as being 5x the largest droplet dimension according to Marchesi *et al*. (2005), and the thickness of the brass substrate 2x the largest droplet dimension. The thermal properties of the 3 regions were considered temperature dependent, and their range was obtained through the Engineering Equation Solver (EES) software library, see Tab. 1.

Table 1. Thermal properties of water and brass.

	Water			Brass	
Temperature [°C]	Density [kg/m³]	Specific heat [J/kg K]	Thermal conductivity [W/m K]	Specific heat [J/kg K]	Thermal conductivity [W/m K]
-196	934.3	742.7	2.786	215.5	52.15
-180	933.8	844.7	2.729	255.8	54.33
-150	932.3	1,040	2.623	304.7	57.59
-120	930.3	1,242	2.516	332.7	61.12
-90	927.7	1,449	2.41	352.4	64.83
-60	924.6	1,663	2.303	363.5	68.65
-30	920.9	1,882	2.197	369	72.49
-10	918.1	2,056	2.125	370.1	73.76
0	1000	4,228	0.5475	371.2	75.02
5	1000	4,200	0.5576	371.7	75.65
10	999.7	4,188	0.5674	372.3	76.27
15	999.1	4,184	0.577	373.2	76.89
20	998.2	4,183	0.5861	374.3	77.5
25	997.1	4,183	0.5948	377	78.72
30	995.7	4,183	0.603	380.3	79.82

Despite showing a smaller variation, the properties of air were also considered dependent on temperature, varying the density, thermal conductivity and specific heat for the same temperature range shown in Tab. 1. The enthalpy of fusion for water is a value constant of 333.6 kJ/kg, with phase change (solid-liquid) around 0 °C. The density of brass is a fixed value of 8605 kg/m³. Air and water viscosities were considered constant, with values of 1.7894x10-05 kg/m.s and 0.001003 kg/m.s, respectively.

3.1 Computational Mesh Analysis

The ANSYS mesh® was used to create the computational meshes, applying the GCI - Grid Convergence Index method, presented by Celik *et al*. (2008), for their evaluation. Three meshes were created, with a refinement ratio of $r_{1\text{-}2}$ = 1.5 and $r_{2\text{-}3}$ = 1.3, with 35.784 elements, 81.038 elements and 136.481 elements. The reference parameter used for mesh refining was drop solidification, defined by its mass fraction (β). Table 2 presents the values found in the evaluation of the quality of the meshes using the GCI method.

Table 2. Mesh quality information.

Mesh	Element size [m]	Nº of elements	Orthogonal quality [-]	Skewness [-]
1	2.610×10^{-5}	35784	0.99271	0.00599
2	1.174×10^{-5}	81038	0.99100	0.00603
3	1.334×10^{-5}	136481	0.99101	0.00611

A value for the mesh convergence index was obtained relating meshes 1 and 2 of $GCI_{2\text{-}1}$ = 0.228% and of $GCI_{3\text{-}2}$ = 0.234% for meshes 2 and 3. Both values are within acceptable limits in the literature of up to 5%. Thus, mesh 2 was used to compare the numerical-experimental results. Fig. 8 shows the refinement of the meshes used in the GCI analysis.

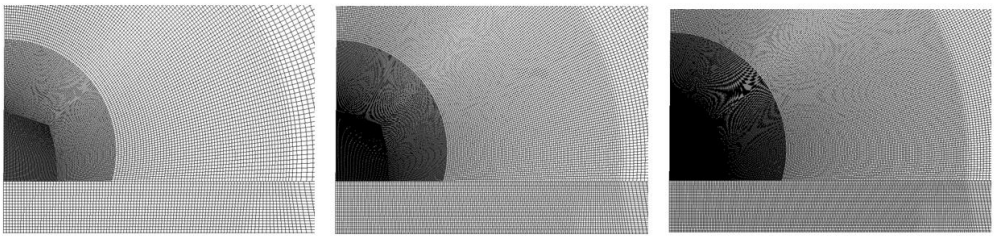

Mesh 1 Mesh 2 Mesh 3

Figure 8. Numerical meshes used in GCI calculation.

3.2 Numerical Simulation Setup

The computer simulations were performed using the solidification model present in the ANSYS Fluent® software, with its energy equation written in terms of enthalpy, as shown by Eq. (1).

$$\frac{\partial}{\partial t}(\rho H)+\nabla\cdot(\rho\vec{v}H)=\nabla\cdot(k\nabla T)+S \tag{1}$$

where H is the phase enthalpy, k is the thermal conductivity, ρ is the density, v is the fluid velocity and S is the source term. The continuity and momentum equations employed by the software are described by Eq. (2) and Eq. (3).

$$\frac{\partial\rho}{\partial t}+\nabla\cdot\left(\rho\vec{V}\right)=0 \tag{2}$$

$$\frac{\partial\rho\vec{V}}{\partial t}+\nabla\cdot\left(\rho\vec{V}\vec{V}\right)=-\nabla p+\nabla\cdot\left(\mu\nabla\vec{V}\right)+\rho\vec{g}+S \tag{3}$$

The source term S for the case of solidification is determined according to Eq.04.

$$S=\frac{(1-\beta)^2}{(\beta^3+\varepsilon)}A_{mush}\cdot\vec{V} \tag{4}$$

where β is the liquid mass fraction, ε is too small a value to avoid division by zero and A_{mush} and is a constant at the solid-liquid interface.

The total time simulated was 20 seconds, with a time-step size of 0.005 seconds. In the simulation setup, a laminar viscosity model, SIMPLE discretization method to solve the pressure-velocity coupling and second order algorithms for pressure, energy, momentum and transient formulation were used. The convergence criterion defined in relation to the residuals was $1x10^{-8}$ for energy and $1x10^{-6}$ for the other variables, and in relation to the number of interactions, it was 1.000 interactions per time step.

4. RESULTS AND DISCUSSION

Fig. 9 shows the experimental and numerical temperature curves performed by CFD computer simulation using ANSYS Fluent® software. The experimental values were close to each other, reaching a minimum temperature in the range of -160 °C to -180 °C in a total time of 20 seconds, except for experimental curve 4 which reached minimum values around -140 °C for the same time step. The experimental curves 1, 2, 3 and 4 obtained similar values for the cooling rate during the solidification process, with values of 567.97 °C/min, 600.34 °C/min, 647.36 °C/min e 551.90 °C/min, respectively. Experimental curves 5 and 6 achieved higher cooling rates than others, with values of 865.97 °C/min for curve 5 and 832.63 °C/min for experimental curve 6. This difference between the values of the cooling rate can be explained by the temperature measurement position and the variation in the contact angle of the droplet with the cooling surface, where the deviation found during measurements was 11.37°, causing the variation of the effective droplet contact angle between 63.14° and 85.88°.

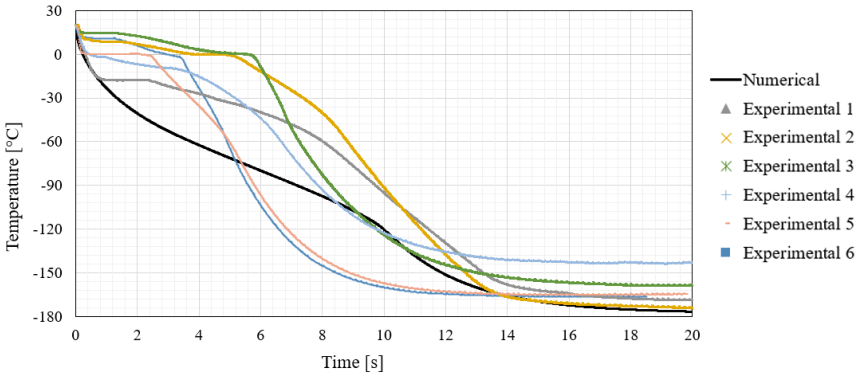

Figure 9. Numerical and experimental curves of temperature for the vitrification process.

In the computational simulations, it was possible to reach average temperatures between -170 °C and -180 °C in a time step of 20 s, with average cooling rate of 589.92 °C/min and complete solidification of the droplet in 9.965 s, as illustrated by Fig. 10.

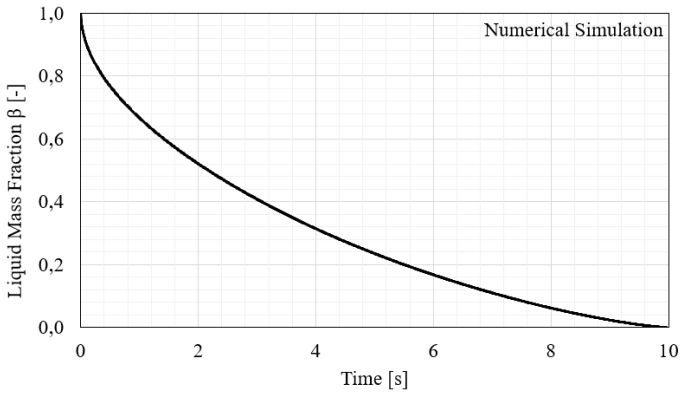

Figure 10. Solidification curve performed by numerical simulation.

A good agreement between the numerical result and the experimental results of curves 1 - 4 (average cooling rate of 591.8 °C/min), can be seen, with a relative difference of 0.33%. Regarding curves 5 and 6, the difference between the average of the experimental and numerical cooling rate was 30.54%, due to the discrepancy between the experimental and simulated contact angles and the position of the temperature measurement.

From the graph shown in Fig. 9 it is possible to verify that the numerical temperature curve differs from the pattern presented by the experimental curves, which tend to stabilize the temperature at the beginning of the freezing process, around 0 °C. This is due to the temperature measurement position inside the droplet, where in the computer simulation the average temperature was considered as a reference. Fig. 11 shows the temperature dependence in relation to the measurement position inside the droplet, through computer simulation, dividing the droplet height into 9 points.

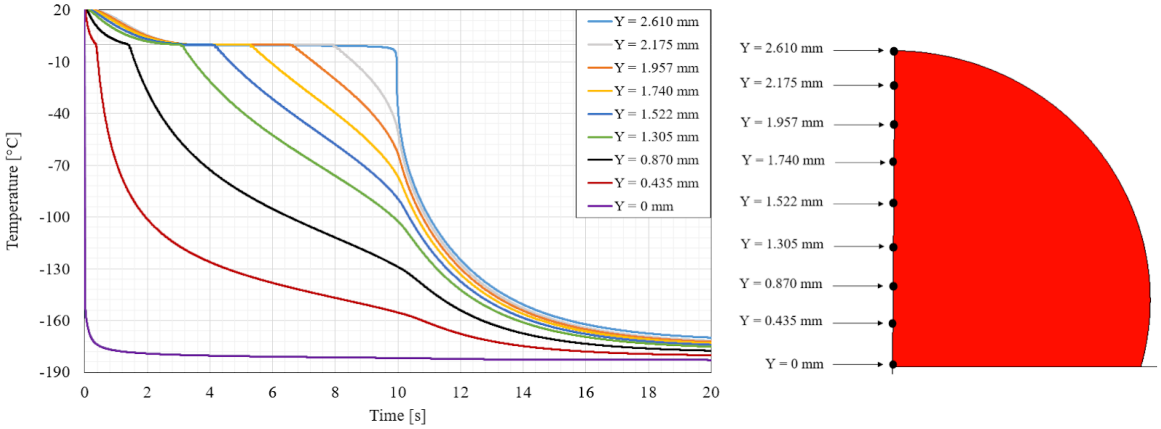

Figure 11. Temperature behavior in relation to the measurement position.

Taking the temperature at specific points, the similarity of behavior between the numerical-experimental temperature curves is verified. The behavior of the temperature curve can be divided into 4 regions: pre-freezing region, stabilization region, rapid freezing region and post-freezing region, see Fig. 12, where in regions further away from the cooling surface the perception of the divisions is better represented.

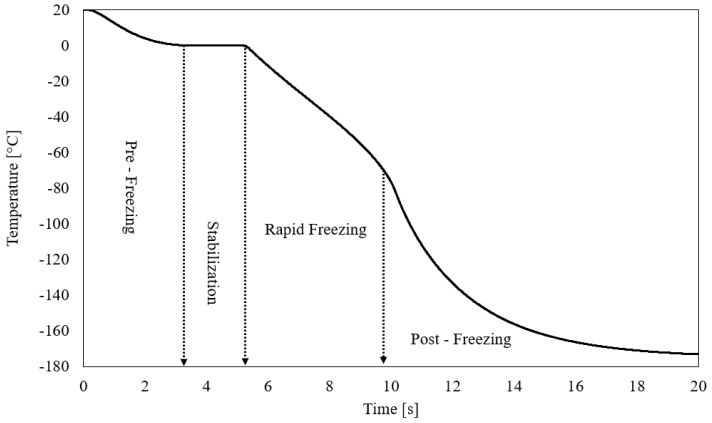

Figure 12. Temperature curve regions during the freezing process.

The limits of the regions will vary depending on the temperature measurement position, where regions closer to the cooling surface have a shorter stabilization time. The behavior of the dripping vitrification process can also be observed through the temperature and solidification contours, as shown in Fig. 13 and 14.

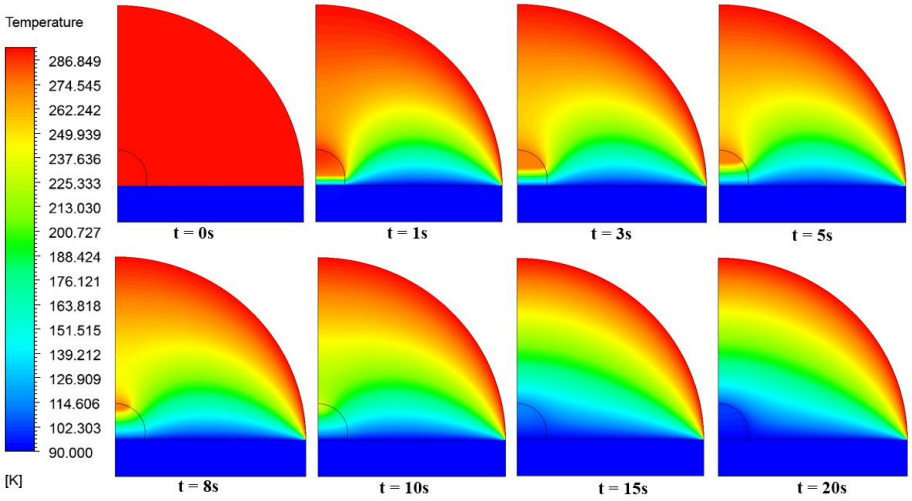

Figure 13. Contours of temperature during the vitrification process.

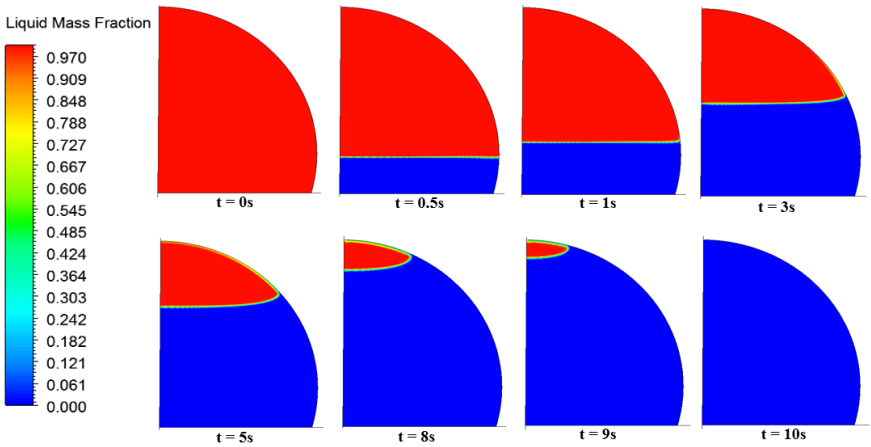

Figure 14. Contours of droplet solidification (liquid mass fraction of water) during the vitrification process.

Through the Fig. 13 and 14, it is possible to verify the behavior of the solidification of the droplet, completely solidifying in less than 10 s, as well as the temperature of the droplet, the substrate, and the environment. The computational simulation resource is a powerful tool to assist in experiments with high complexity phenomena involved, providing detailed information on regions of great interest.

5. CONCLUSION

The numerical-experimental results presented in this work showed good agreement between them, where a difference of only 0.33% was obtained for the cooling rate between the simulation and the experimental curves 1 - 4, with values of 589. 9 °C/ min and 591.8 °C/min, respectively. The large difference in values for the cooling rate of the simulation with experimental curves 5 and 6 (30.54%) is related to the position of the temperature measurement and the variation in the contact angle, varying 11.37°, where higher contact angle values provide greater cooling rates, and vice versa. The numerical temperature curve showed a steeper curve behavior than the experimental curves, which may be related to the nature of experimental tests, such as temperature measurement method and position, drop height, contact angle variation and environmental conditions tests such as temperature and humidity.

Despite the discrepancies in values, it was possible to replicate numerically the experiments carried out, observing with a detail the contact droplet vitrification process, as well as the solidification rate, which would not be possible to obtain experimentally with good accuracy. Through computer simulations it will be possible to replicate different test conditions, seeking the improvement and development of new vitrification processes. For future work, it is intended to modify the experimental bench, controlling more rigorously the external conditions, such as environment temperature, humidity, drop height, temperature measurement and data acquisition system. It is also intended to carry out new computational simulations increasing the degree of phenomena involved, such as including environment humidity, mixing of cryoprotectant substances, modification of sample volume and application of cellular materials.

6. REFERENCES

Akiyama, Y., Shinose, M., Watanabe, H., Yamada, S. and Kanda, Y., 2019. “Cryoprotectant-free cryopreservation of mammalian cells by superflash freezing”. In *Proceedings of the National Academy of Sciences of the United States of America*, Vol. 116, No. 16, pp. 7738–7743.

Bahari, L. et al. “Directional freezing for the cryopreservation of adherent mammalian cells on a substrate”. *PLOS ONE*. p. 1–17, 2018.

Celik, I. B. et al. “Procedure for estimation and reporting of uncertainty due to discretization in CFD applications”. *Journal of Fluids Engineering, Transactions of the ASME*, v. 130, n. 7, p. 0780011–0780014, 2008.

Dupesh, S.; Gunasekaran, K. “A simple method of human sperm vitrification”. *MethodsX*. v. 6, p. 2198–2204, 2019.

Li, Y. et al. “Microencapsulation Facilitates Low-Cryoprotectant Vitri fi cation of Human Umbilical Vein Endothelial Cells”. *ACS Biomaterials Science & Engineering*, v. 5, p. 5273–5283, 2019.

Marchesi, R., Maffè, M. and Moraschi, M., 2005. “Computational fluid dynamics analysis of cell cooling process”. *Cell Preservation Technology*, Vol. 3, No. 4, pp. 229–237.

O’Neill, H. C., Nikoloska, M., Ho, H. T., Doshi, A., & Maalouf, W. 2019. “Improved cryopreservation of spermatozoa using vitrification: comparison of cryoprotectants and a novel device for long-term storage”. *Journal of Assisted Reproduction and Genetics*, 36(8), 1713–1720. https://doi.org/10.1007/s10815-019-01505-x.

Santin, T. R., Blume, H., Mondadori, R. G., 2009. “Conservação de embriões – metodologias de vitrificação”. *Veterinária e Zootecnia*, Vol. 16, No. 4, pp. 561-574.

Shi, M. et al. “High-Throughput Non-Contact Vitrification of Cell-Laden Droplets Based on Cell Printing”. *SCIENTIFIC REPORTS*, v. 5, 2015.

Su, F., Zhao, N., Deng, Y. and Ma, H., 2018. “An ultrafast vitrification method for cell cryopreservation”. Transactions of the ASME *Journal of Heat Transfer*, Vol. 140, No. 1, pp. 1-4, 2018.

Tiersch, C. J. et al. 3-D printed customizable vitrification devices for preservation of genetic resources of aquatic species. Aquacultural Engineering, v. 90, n. May, p. 102097, 2020.

Vajta, G., Holm, P., Kuwayama, M., Booth, P.J., Jacobsen, H., Greve, T. and Callesen, H., 1998. “Open pulled straw (OPS) vitrification: A new way to reduce cryoinjuries of bovine ova and embryos”. *Molecular Reproduction and Development*, Vol. 51, No. 1, pp. 53-58.

Vries, R. J. DE et al. “Bulk Droplet Vitrification: An Approach to Improve Large-Scale Hepatocyte Cryopreservation Outcome”. *Langmuir*. v. 32(23), p. 7354-7363, 2019.

Zhang, Y. et al. “Isochoric vitrification: An experimental study to establish proof of concept”. *Cryobiology*, v. 83, n. May, p. 48–55, 2018.

Zhao, G.; FU, J. “Microfluidics for cryopreservation”. *Biotechnology Advances*, v. 35, p. 323–336, 2017.

Zhou, X. et al. “Investigation on the thermal performance of a novel microchannel-aided device for vitrification of cells/tissues” *Applied Thermal Engineering*, v. 119, p. 189–196, 2017.

7. RESPONSIBILITY NOTICE

The authors are the only responsible for the printed material included in this paper.